Unraveling the Reaction Mechanism for Nickel-Catalyzed Oxidative Dehydrogenation of Ethane by DFT: The C−H Bond Activation Step and Its Following Pathways

Xufeng Lin,[*,†,‡,§] Yanyan Xi,[†,∥] and Jian Sun[⊥]

[†]State Key Laboratory of Heavy Oil Processing, [‡]Key Laboratory of Catalysis of China National Petroleum Corporation, [§]College of Science, and [∥]College of Chemical Engineering, China University of Petroleum (East China), Qingdao, P. R. China, 266555

[⊥]Department of Chemistry, The University of Hong Kong, Pokfulam Road, Hong Kong, P. R. China

S *Supporting Information*

ABSTRACT: Understanding the reaction mechanism for oxidative dehydrogenation (ODH) of alkanes, especially the key intermediate(s) that generates alkene is essential for designing good ODH catalysts. To unravel the mechanisms for Ni-based oxide-catalyzed ODH reactions, we investigated the reactions of C_2H_6 with Ni_3O_x ($x = 1, 2, 3$) clusters by density functional calculations. For Ni_3O_3, three pathways were examined for the C−H bond activation step, and the one with concerted mechanism undergoing at two sites is the most favorable pathway, producing an ethylnickel species. Then, four reaction pathways, namely, β-H elimination, α-H abstraction, C−C bond cleavage, and isomerization to an ethoxide species, with 11 reaction channels, were examined to understand the behavior of this ethylnickel species. The selectivity of C_2H_4 (S_{C2}) for this reaction was calculated based on the relative rates of these four pathways. Similar investigations were carried out on the reactions of Ni_3O_2 and Ni_3O_1 clusters with C_2H_6. The calculated S_{C2} increases from ∼37 to over 99% with decreasing x value in Ni_3O_x.
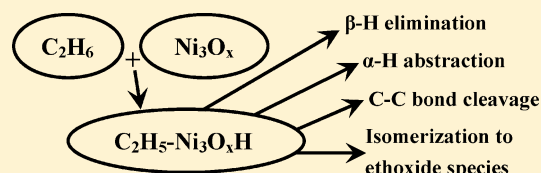
1. INTRODUCTION

Selective conversions of light alkanes to molecules with functional groups are of great industrial and fundamental interest, especially nowadays because the oil price remains at a high level and oil depletion in three to five decades is widely expected. Oxidative dehydrogenation (ODH) of light ($C_2 \sim C_4$) alkanes provides an attractive alternative to the present methods for production of alkenes.[1−3] The key problem for the industrial application of ODH is still the unavailability of catalyst presenting desired selectivity to alkene with high conversion of alkane. Great efforts for seeking such catalyst have been made for several decades.[1] However, the reaction mechanisms for catalytic ODH reactions are still elusive in the literature.[2,3] Most ODH works emphasize in catalytic reaction tests, whereas many fewer concerns have been taken in reaction mechanism,[4−10] especially on the molecular level.[11] This is partially due to the short lifetime of the surface intermediate(s) involved during the oxidation of alkane by metal oxides and the reoxidation of reduced metal site(s) by oxidants. Several key questions about the detailed ODH mechanism are poorly understood, such as: (Q1) what is the primary intermediate(s) after the C−H bond activation of alkane on a catalyst,[2,3] (Q2) what is the reaction behavior of this intermediate(s), (Q3) how does the structure of active site effect the type and the reaction behavior of the intermediate(s), and (Q4) how does one increase the concentration of the active site(s), which favors the intermediate(s) kinetically leading to high selectivity of alkene on a catalyst?

Obviously the answers to the above questions are essential for designing good ODH catalysts. Quantum chemical, especially density functional theory (DFT)[12−21] calculation, provides powerful tools for understanding a reaction system on the molecular level. Presently, in most of the DFT studies dealing with the ODH reaction,[14−16,19,20] the models for catalyst are single-crystal surfaces. However, a huge gap exists between the well-defined single-crystal surfaces and the surfaces of most solid catalysts, in that typically the latter contain ill-defined metal/metal oxide clusters, the size of which range from subnanometer to ∼50 nm. Therefore, using metal oxide cluster models seems to be more plausible than using single-crystal models for the active sites in heterogeneous catalysis,[21−23] which could be even more right when dealing with the active sites of around or less than 1 nm (subnanometer). Subnanometer materials were found to possess catalytic properties not observed in their large-size analogues, and subnanometer catalysts may have attractive properties in catalysis.[24,25] DFT calculations using cluster models will help researchers better understand the field of catalysis with subnanometer catalysts.

This work aims at seeking the answers for questions Q1 and Q2 proposed in the first paragraph for Ni-catalyzed ODH reaction of ethane (ODHE). Although V[26−28] and Mo[4,29,30] are the most extensively studied metals for ODH, in the recent
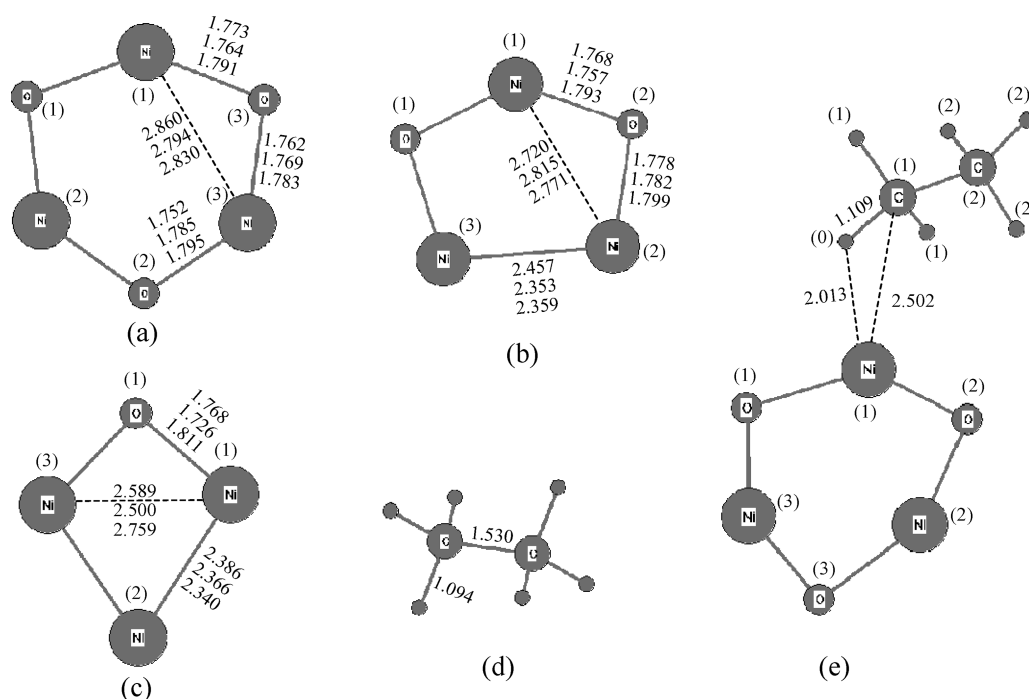
Figure 1. Ni_3O_3 (a), Ni_3O_2 (b), and Ni_3O_1 (c) models, C_2H_6 molecule (d), and the reactant complex of a C_2H_6 molecule with a Ni_3O_3 cluster in heptet state (e). Key distances are indicated in angstroms. The three stacking numbers from top to bottom are the distances in triplet, quindruplet, and heptet states, respectively. Geometry optimizations were done on the B3LYP/BS1 level, which will not be indicated hereafter in this Article.

years Ni-based catalysts were found to present good yield of ethylene[31−41] in the ODHE reactions, and some reports for using Ni catalysts for ODH of propane[42,43] can also be seen in the literature. For example, ODHE catalyzed by NiO-loaded high-surface-area MgO was examined by Nakamura and coworkers,[39] and a C_2H_6 conversion of 68.8% and a C_2H_4 selectivity of 52.8% were achieved at 600 °C. Ni-loaded H−Y catalyst giving a productivity of C_2H_4 over 1 $g_{C2}g_{cat}^{-1}$ h^{-1} at 600 °C was reported by our group.[36] Catalyst giving a productivity of C_2H_4 smaller than this value is unlikely to be interested by industrial investors.[1]

In this work, DFT calculations were carried out to characterize the potential energy surfaces (PESs) of the reactions between Ni_3O_x ($x = 1,2,3$) clusters and C_2H_6 to understand the key steps in Ni-catalyzed ODH reactions. The aim of this work is to shed light on the fate of an alkane molecule when encountered with metal oxide by examining different pathways of the C−H bond activation step (denoted as the first step in this Article) and the fate of the intermediate generated from the first step by examination of different pathways of bond cleavage for this intermediate (denoted as the second step). We found the reaction rate of the β-H elimination pathway relative to the sum of rates for all pathways in the second step, which determines the product selectivity of ethylene (S_{C2}) for a certain reaction. S_{C2} can be associable with the initial selectivity of ethylene (S_0) in a catalytic ODHE reaction. Our results provide a new insight into the intermediate(s) involved in transition metal-catalyzed oxidation of light alkanes. A discussion on how to design good ODH catalysts is given based on the conclusions.

2. COMPUTATIONAL METHODS AND THE MODELS OF NI_3O_X CLUSTERS

DFT calculations were performed by employing the hybrid B3LYP[44−46] exchange and correlation functionals to explore the PESs of the reaction between C_2H_6 and Ni_3O_x ($x = 1, 2, 3$) clusters. B3LYP is known to provide a good description of the PES for the transition-metal oxide clusters.[21,47] All of the PESs were examined by optimizing geometries in the energy minimums for the reactants, the intermediates, and the products and the first-order saddle points for transition states using the Gaussian 03 program suite.[48] Frequency analyses were performed to confirm energy minimums and first-order saddle points as well as to obtain the zero-point corrected energies (ZPEs), entropies, and free energies (at 298.15, 823.15, and 873.15 K) of the optimized geometries. The temperature mainly concerned is 873.15 K. The 6-311G** basis set was used for all C, H, O atoms, and the Stuttgart basis set was used for the Ni atoms. Five component d functions were employed in the calculations. These basis sets are denoted as BS1 in this Article.

The results reported in our previous papers[35,36] indicate that several first-row transition-metal-loaded Y zeolites (M/Y) may exist in quite small clusters because no features relating to M can be observed on the X-ray diffraction patterns, whereas elemental analysis shows significant metal loadings. The ex situ EXAFS (extended X-ray absorption fine structure) spectroscopic study shows that the Ni components in Ni/HY can be represented as $NiO\cdot Ni_y$[36] when Ni/HY is exposed to a fuel-rich reaction mixture of ethane, O_2, and He. Therefore, it is reasonable to expect that the active sites on Ni-loaded zeolite catalyst are small $NiO\cdot Ni_y$ clusters. Therefore, the Ni_3O_x ($x = 1$, 2, 3) clusters were used to model the nickel oxide clusters on the catalytic supports such as zeolites. The optimized geometries of Ni_3O_3, Ni_3O_2, and Ni_3O_1 are presented in Figure 1a−c.

Metal oxide clusters may have different spin multiplicities close in energy.[21] For the reactions involving the Ni_3O_3 and Ni_3O_2 clusters, only the reaction pathways with triplet, quindruplet and heptet states will be presented in this paper,
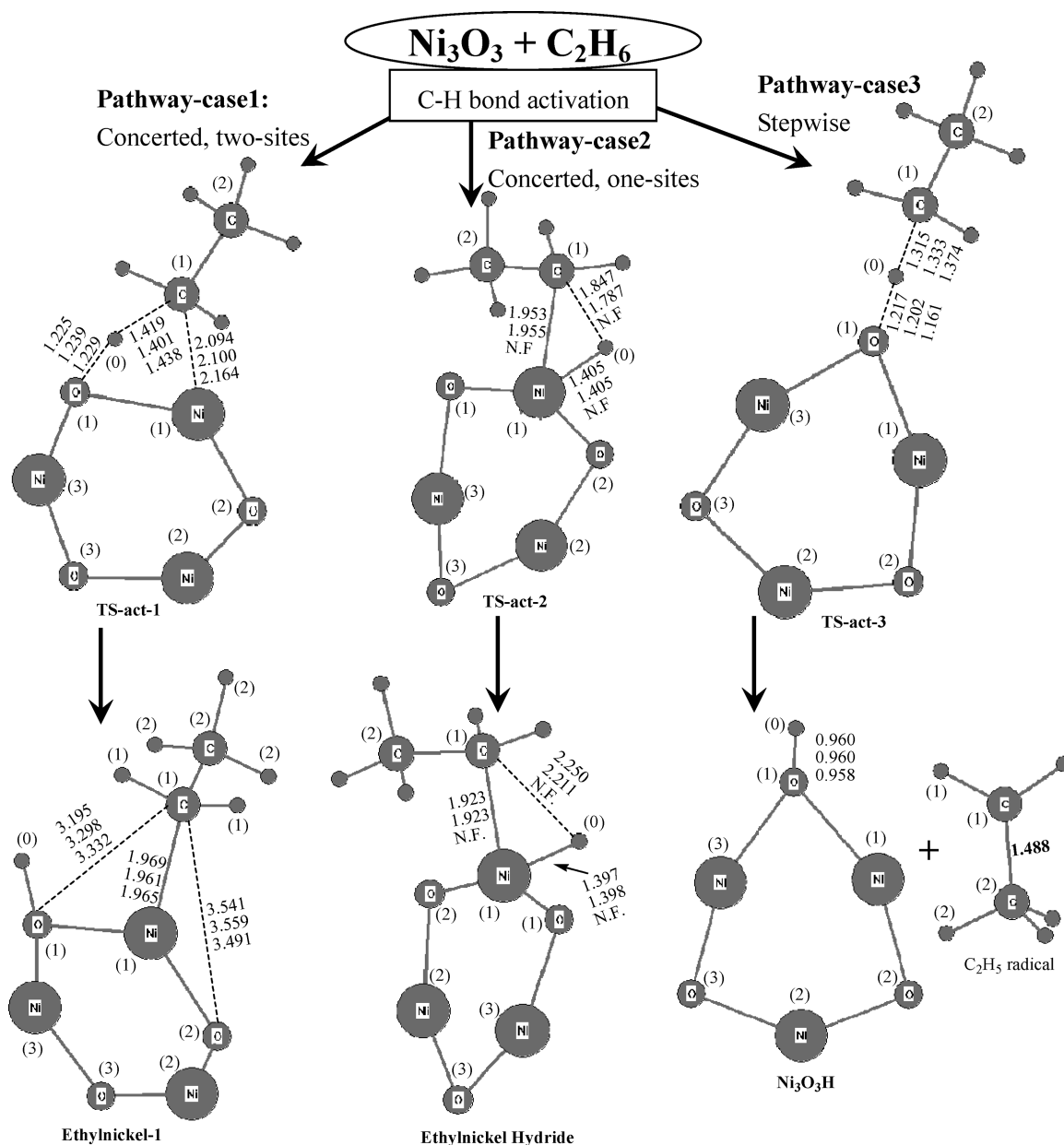
Figure 2. Optimized geometries for the transition states and product complexes or separated products for three pathways examined in the C−H bond activation step for the reaction of Ni_3O_3 with C_2H_6. Key distances are indicated in angstroms. The three stacking numbers from top to bottom are the distances in triplet, quindruplet, and heptet states, respectively. "N.F." stands for "not found".

since the energies of the relating species with singlet and nonet states are much higher than those with trieplet, quindruplet and heptet states. For the reactions involving the Ni_3O_1 cluster, only the reaction pathways on triplet and quindruplet PESs will be reported because the energies of the relating species with singlet, heptet, and nonet states are much higher than those with triplet and quindruplet states.

3. RESULTS AND DISCUSSION

3.1. First Step of Ni_3O_3 Case: C−H Bond Activation of C_2H_6. The C−H bond activation was extensively studied for either homogeneous[49−51] or heterogeneous catalysis.[22,23,52] The main target of this section is to understand question Q1, as described in the Introduction, for the cases of using nickel oxide as ODH catalyst.

For C_2H_6 reacting with Ni_3O_3, heptet $Ni_3O_3 + C_2H_6$ was chosen as the starting material (**SM**), and the energy or free energy of **SM** was selected as the reference. Molecular adsorption of C_2H_6 on heptet Ni_3O_3 was first examined by locating the local energy minimum when a C_2H_6 molecule approaches the Ni_3O_3 cluster. The energy minimum appears at the $C(1)\cdots Ni(1)$ distance of ∼2.5 Å (Figure 1e). The energy change of adsorption calculated, for example, for the case of heptet Ni_3O_3 cluster, is −2.9 kcal/mol, which is close to −2.5 kcal/mol for the adsorption of ethane on $V_2O_5(001)$ surface.[15] The entropy loss for the formation of this reactant complex from the separated reactants is 75.3 J·mol^{-1}·K^{-1} at 298.15 K and 113.9 J·mol^{-1}·K^{-1} at 873.15 K. Considered that the OHDE reaction typically undergoes at the temperature range of 600−1000 K, this entropy loss results in a more stable state in the gas phase than being adsorbed on the metal oxide surface.
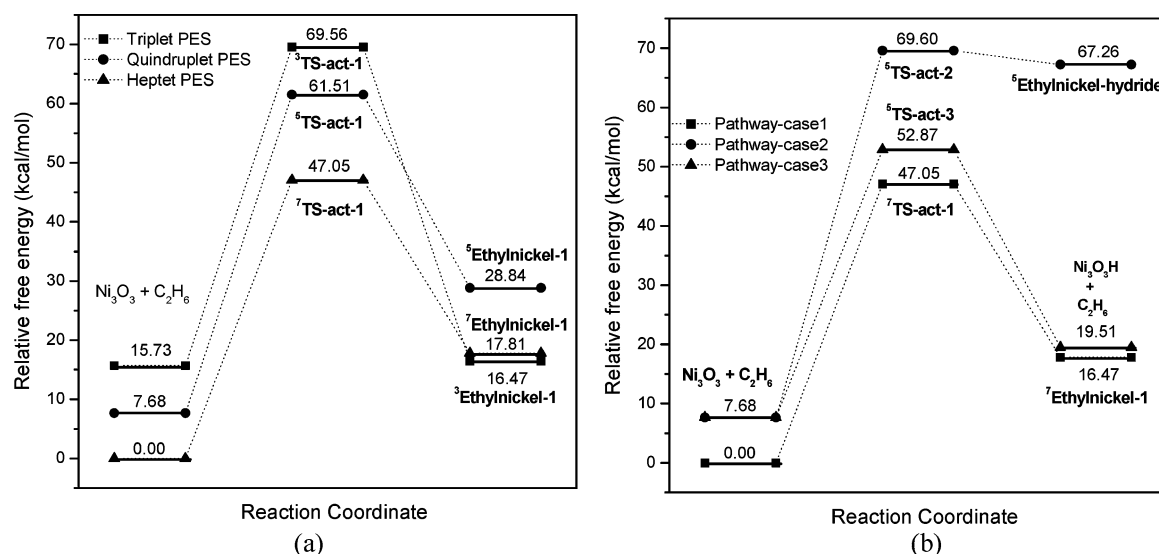
Figure 3. Relative free energy (at 873.15 K) profiles for the C−H bond activation step in C_2H_6 reacting with Ni_3O_3. The free energy of heptet Ni_3O_3 + C_2H_6 is the reference. (a) Free-energy profiles for **pathway-case1** on triplet, quindruplet, and heptet PESs. (b) Three pathways with their lowest free energy of activations.

Therefore, it is reasonable to conclude that the activation of C−H bond in C_2H_6 is not precursor-mediated.[15] It has been pointed out by some researchers[53] that a more accurate method to calculate the adsorption energy is to use the correlation function including the van der Waals force instead of B3LYP for the adsorption of alkane on metallic surface. However, considering the case that the typical temperature for desorption of alkane from metallic surface is under 200 K,[54] the above conclusion is still plausible.

The C−H bond activation step of alkanes on metal oxides may undergo with different mechanisms,[22] which can be divided into two categories: concerted and stepwise mechanisms. In the concerted mechanism, the cleavage of the C−H bond is accompanied by the formation of two new bonds. For the case of C−H bond activation on Ni_3O_3, the C(1) and H(0) atoms (Figure 1e) may form new bonds with one O site, with one Ni site, or with two sites. Although many attempts were performed by considering all possible combinations, the transition-state structures of only two reaction pathways, namely, **pathway-case1** and **pathway-case2**, were found for the concerted mechanism. (See Figure 2.) For **pathway-case1**, the C(1)−H(0) bond cleavage is accompanied by the formation of the H(0)−O(1) and C(1)−Ni(1) bonds, which can be seen from the changes of atom distances from **SM** to the transition state, **TS-act-1**, and to the product, **Ethylnickel-1** species, as shown in Figure 1a,d and the left two panels of Figure 2. For **pathway-case2** (Figure 2), both of the C(1) and H(0) atoms attack the Ni(1) site, and the C(1)−Ni(1) and H(0)−Ni(1) bonds are formed in the product of the C−H bond activation step.

For the stepwise mechanism, only one pathway (**pathway-case3** in Figure 2) was found, where the cleavage of C(1)−H(0) bond is accompanied by the formation of H(0)−O(1) bond. Different from the cases of **pathway-case1** and **pathway-case2**, two separated products are produced: a Ni_3O_3H and an ethyl radical. The combination of this two separated products to form a further product complex was not examined.

The free energy of activation ($\Delta G\ddagger$) needed for different pathways may be different, and if one pathway has an obviously lower $\Delta G\ddagger$ than other pathways have then this pathway can be the dominant one for the C−H bond activation step. Figure 3a shows the relative free-energy profiles for **pathway-case1** with triplet, quindruplet, and heptet states, respectively. $\Delta G\ddagger$ for the heptet state (47.1 kcal/mol at 873.15 K) is the lowest in the three spin multiplicities for **pathway-case1**. Figure 3b shows that the lowest $\Delta G\ddagger$ for **pathway-case2** is 69.6 kcal/mol, and the lowest $\Delta G\ddagger$ for **pathway-case3** is 52.9 kcal/mol with all spin multiplicities examined. These data bring the answers of the following two important questions for the C−H bond activation step: (1) what is the contribution of a certain spin multiplicity to a given pathway and (2) what is the contribution of a certain pathway to the overall C−H bond activation step?

In general, for two parallel pathways that share a same reactant or if the reactants of which are easier to change to each other than go to the transition states, the relative reaction rate of these two pathways can be determined by the Boltzmann distribution[55] of their corresponding transition states, which can be written as

$$r_2/r_1 = \exp\left(\frac{G_{TS1} - G_{TS2}}{RT}\right) \qquad (1)$$

where G_{TS} is the free energy of a transition state relative to an arbitrary reference. By applying the data in Figure 3a to eq 1, one can obtain that for **pathway-case1** $r_{triplet}/r_{heptet} = 2.3 \times 10^{-6}$ and $r_{quindruplet}/r_{heptet} = 2.4 \times 10^{-4}$ at 873.15 K. So for the **pathway-case1**, the reaction undergoes with the heptet state dominantly, and the contribution of other spin multiplicities can be discarded. Similar conclusions can be drawn for **pathway-case2** and **pathway-case3**; that is, only one spin multiplicity dominates each pathway, and the contributions of other spin multiplicities are trivial.

Some readers may argue about the validity of the above conclusion from eq 1 when concerning that sometimes the conversion between different spin multiplicities for a species may be "spin-forbidden"; therefore, the reaction rates with different spin multiplicities should be calculated independently. To understand how spin state influences the above conclusions made from eq 1, we calculated the energies of Ni_3O_3 with different multiplicities with a same geometry. It was found that

Scheme 1. Four Reaction Pathways Including Different Channels Examined for Ethylnickel-1^a

(a) β-H elimination:
CHAN-β-p

(b) α-H abstraction:
CHAN-α-p

(c) C–C bond cleavage
CHAN-cle-p

(d) Isomerization
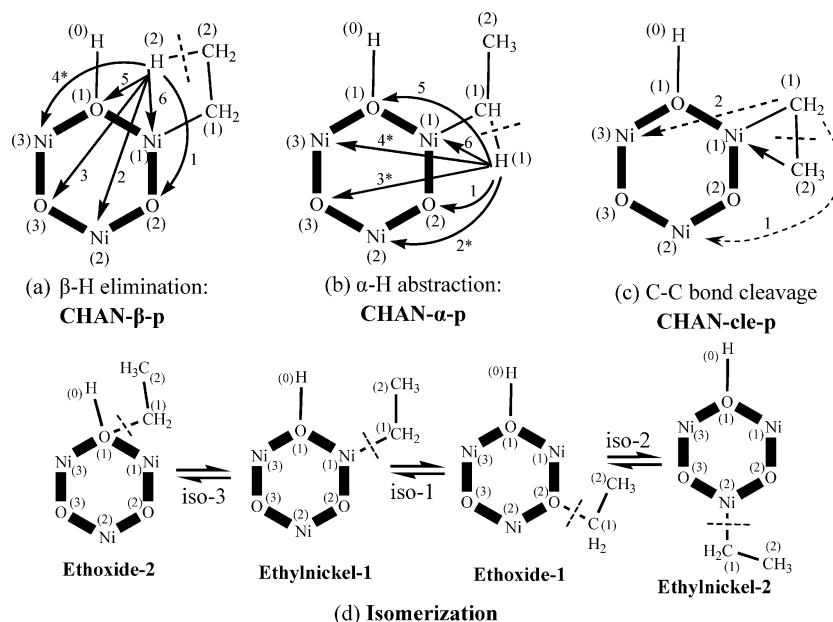
^{a}Number in the parentheses represents the atomic label. The number near the arrow represents the channel number (p value) for a certain pathway in panels a–c, where the number with a star represents the corresponding channel that was not found in this work. In panel d, iso-1 and iso-3 are the two isomerization channels for **Ethylnickel-1**, and iso-1 and iso-2 are the two isomerization channels for **Ethoxide-1**.

for the same Ni$_3$O$_3$ geometry (optimized geometry with heptet state, see Figure 1a), the free-energy difference between a heptet and a quindruplet state ($G_{heptet} - G_{quindruplet}$) is 11.3 kcal/mol. The $G_{heptet} - G_{triplet}$ and $G_{quindruplet} - G_{triplet}$ values are 19.4 and 8.1 kcal/mol, respectively. The data obtained in this way are definitely larger than the exact value of the minimum energy needed for spin conversions, obtaining which requires a full scan of PESs. However, they are still enough to conclude that the spin conversion between different multiplicities is much faster than the C–H bond activation step because the energy needed for the spin conversion (<20 kcal/mol) is much smaller than that needed for the C–H bond activation (with the least of 47.1 kcal/mol). This meets the precondition of eq 1. Therefore, in our reaction systems, nearly only one spin multiplicity contributes to a certain pathway, and the relative reaction rate of two certain pathways can be calculated from the corresponding lowest free energy of transition states without considering what the spin multiplicities are.

Using the data in Figure 3b and eq 1, one can obtain that k_{case2}/k_{case1} is 8.8×10^{-6} and $k_{case3}/k_{case1} = 0.035$. That is to say, for the C–H bond activation step, the contribution of the radical mechanism is little, and that of the pathway where the C and H atoms attack a same site is even less. As can be seen in the lower-left panel of Figure 2, an ethylnickel species (denoted as **C$_2$H$_5$-Ni$_3$O$_3$H**, simply **Ethylnickel-1** in this Article) can be identified in the product of the main pathway (**pathway-case1**) for the C–H bond activation step. Therefore, it can be anticipated that the reaction behavior of **Ethylnickel-1** determines the initial selectivities of different oxidation products for the whole oxidation reaction of ethane with nickel oxides. A systematic investigation of four reaction pathways with several reaction channels was carried out for **Ethylnickel-1**, and the results are presented in Section 3.2.

3.2. Second Step of Ni$_3$O$_3$ Case: Reaction Behavior of Ethylnickel-1. Compared with the C–H bond activation step for hydrocarbons, the reaction behavior of the intermediate produced from the C–H bond activation step was less studied.[12−21] The main goal for this section is to understand question Q2 in the Introduction for the cases of using nickel oxide as ODH catalyst.

The possible reaction pathways of **Ethylnickel-1** can be elucidated by inspection of the number of types of chemical bond in its Ni–C$_2$H$_5$ moiety. There are four types of chemical bond, that is, the α−C-H [C(1)−H(1)], β−C-H [C(2)−H(2)], C−C [C(1)−C(2)], and Ni−C [C(1)−Ni(1)] bonds in the Ni–C$_2$H$_5$ moiety of **Ethylnickel-1**. (See the lower-left panel of Figure 2 or Scheme 1.) Because the chemical reaction involves bond cleavage, the cleavages of these bonds correspond to the following four reaction pathways, respectively: α-H abstraction, β-H elimination, C−C bond cleavage, and isomerization. (Going back to the starting materials will not be considered here.) All four reaction pathways of **Ethylnickel-1** may undergo with different reaction channels, considering that the detached part may go to different sites. The possible reaction channels for the β-H elimination, α-H abstraction, and C−C cleavage pathways are illustrated in Scheme 1a−c, and the two reaction channels of the isomerization pathway are illustrated in Scheme 1d. For example, in Scheme 1a, the β-H atom [H(2) as indicated] may go to six sites, leading to six possible reaction channels for the β-H elimination pathway. However, for some reaction channels, the transition states and products were not found despite several attempts.

3.2.1. β-H Elimination Pathway. For the β-H elimination pathway, the reaction channels are denoted as **CHAN-β-p**, where $p = 1$−6, as indicated in Scheme 1a. The corresponding transition states are denoted as **TS-β-p**. **CHAN-β-4** was not found, which could account for the less positively charged of the Ni(3) compared with the other Ni site because the ethyl moiety is going to be oxidized when H elimination undergoes. This is verified from the charge analysis. The transition states and products for all other channels are presented in Figure 4.
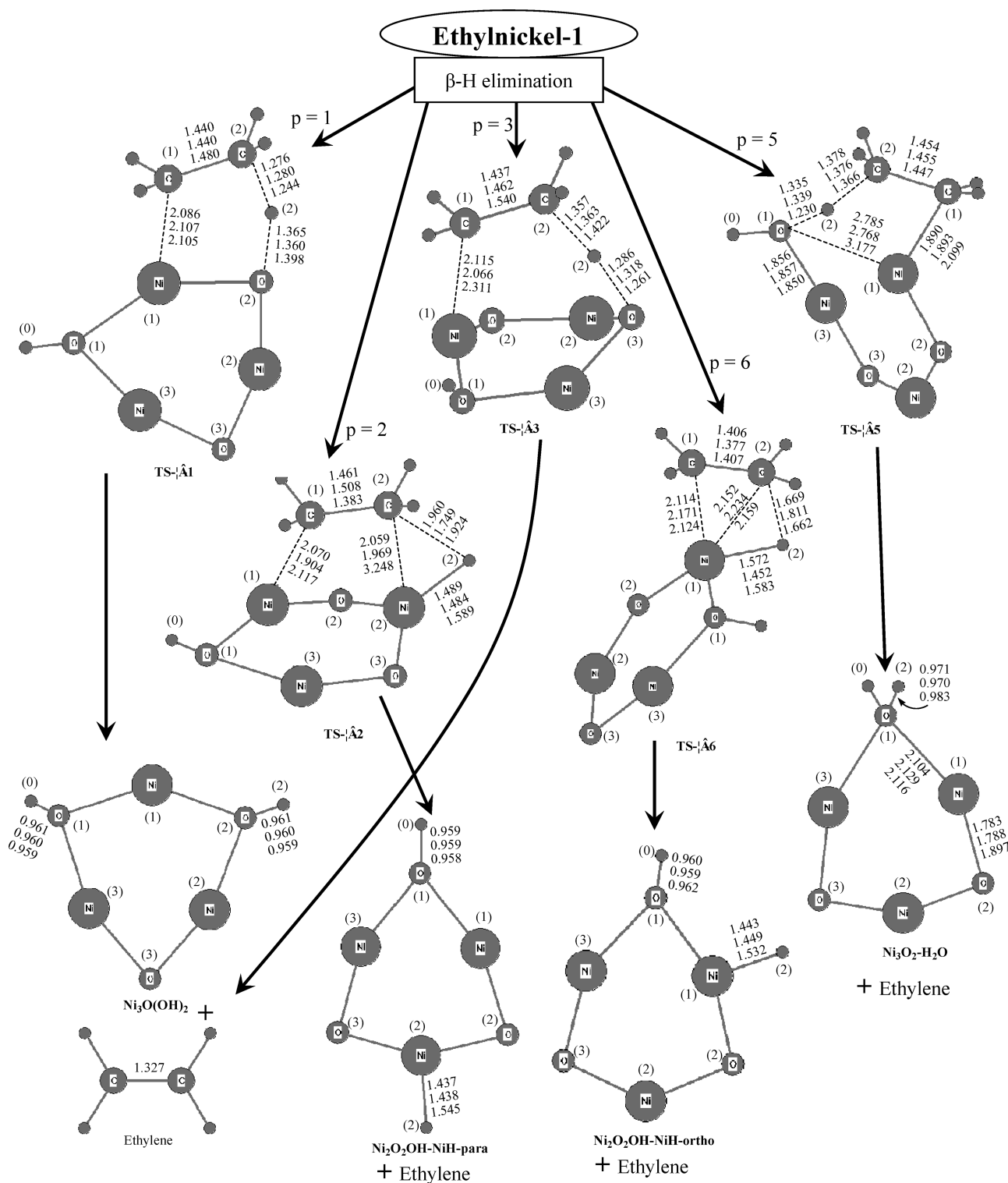
Figure 4. Optimized geometries for the transition states and products for five reaction channels examined for the β-H elimination pathway of **Ethylnickel-1**. Key distances are indicated in angstroms. The three stacking numbers are the distances in triplet, quindruplet, and heptet states, respectively. See Scheme 1a as well.

Comparison of the transition state and product structures of **CHAN-β-1** with that of **Ethylnickel-1**, a clear process of β-H elimination can be identified,[15] with the detachment of C(1) from Ni(1) atom, the detachment of H(2) from C(2) atom, the approaching of H(2) to O(2) atom, and shortening of the C(1)−C(2) bond from a single to double bond length, at the same time. For example, C(2)···H(2) distance increased from 1.091 Å in **Ethylnickel-1** to 1.280 Å in **TS-β-1** in quindruplet (or [5]**TS-β-1**) state, and they are totally detached as in separated products. In **CHAN-β-2**, a trigonal C(2)···H(2)···Ni(2) structure can be seen in the transition-state structure (**TS-β-2**). The C(2)···H(2) distance in **TS-β-2** is larger than that in **TS-β-1**, implicating that the detachment of H(2) from C(2) is more difficult in **CHAN-β-2** than in **CHAN-β-1**. This

F

dx.doi.org/10.1021/jp2088274 | J. Phys. Chem. C XXXX, XXX, XXX–XXX
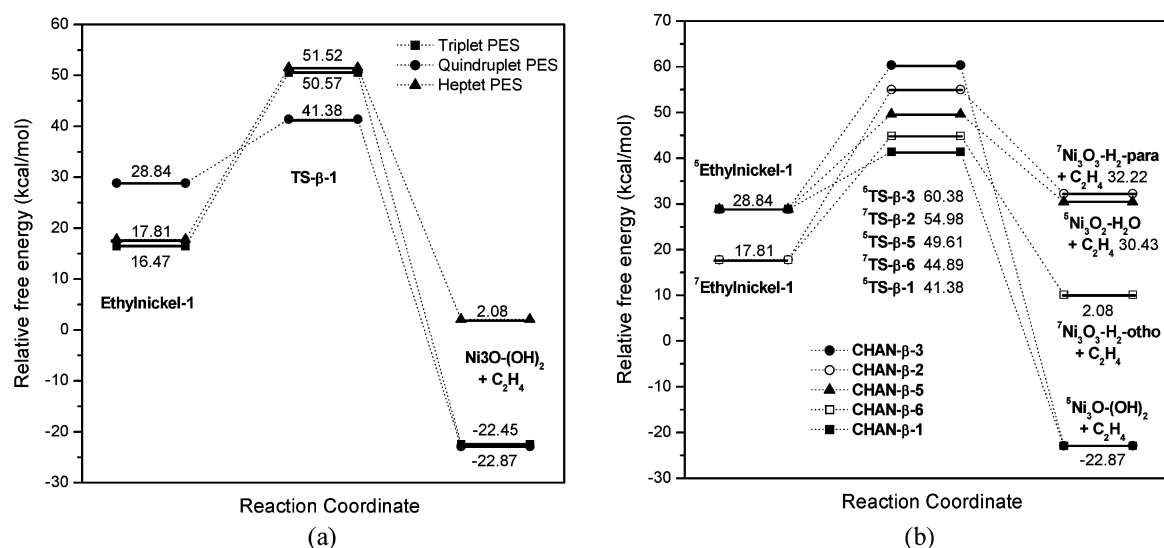
Figure 5. Relative free energy (at 873.15 K) profiles for the β-H elimination pathway of **Ethylnickel-1**. The free energy of heptet $Ni_3O_3 + C_2H_6$ is the reference. (a) Free-energy profiles for **CHAN-β-1** on triplet, quindruplet, and heptet PESs. (b) Five reaction channels with their lowest free energy of activations.

hypothesis is supported in the free-energy profiles shown in Figure 5. Product complexes for **CHAN-β-1** and **CHAN-β-2** are the molecular adsorption of an ethylene molecule on different $Ni_3O_3H_2$ structures. The separated C_2H_4 and $Ni_3O_3H_2$ were found to be more favorable in free energy than the product complexes. Therefore, in all of the reaction channels for the β-H elimination pathway, the structures of product complexes will not be presented in this Article.

The transition state and product structures for **CHAN-β-3** are similar to those for **CHAN-β-1**, as can be seen in Figure 4. In the transition-state structure (**TS-β-5**) for **CHAN-β-5**, the approaching of the H(2) atom to O(1) atom leads to the detachment of O(1) from Ni(1) at the same time. The $Ni_3O_3H_2$ product for **CHAN-β-5** is the adsorption of a water molecule on the Ni_3O_2 cluster. In **TS-β-6** for **CHAN-β-6**, a four-membered-ring feature of $[C(1)\cdots C(2)\cdots H(2)\cdots Ni(1)]$ can be seen, similar to the local structure reported for the dehydrogenation of ethane on GaO^+ ion.[47]

Similar to the questions raised in Section 3.1, now it is important to evaluate the contribution of different spin multiplicity to the rate of a certain reaction channel and the contribution of different reaction channel to the rate of a certain pathway. Figure 5a presents the free-energy profiles for **CHAN-β-1** with the spin multiplicity of triplet, quindruplet, and heptet. Applying the data in Figure 5a to eq 1, one can obtain that $k_{triplet}/k_{quindruplet} = 0.0052$, and $k_{heptet}/k_{quindruplet} = 0.0029$ at 873.15 K, indicating that the triplet and heptet states have trivial contributions to the reaction channel **CHAN-β-1**, which is most favorable to undergo in the quindruplet state.

Similar to the discussion in Section 3.1, because of the spin conversion issue, the above results calculated by using eq 1 are correct only if the energy needed for spin conversion is lower than that needed for the reaction itself. So the energies of heptet and quindruplet **Ethylnickel-1** with the geometry optimized in triplet state were calculated, and the free energies needed for spin conversions between different spin states were found to be no larger than 12.1 kcal/mol. This is much smaller than the free energy of activation for any reaction channels in the β-H elimination pathway (Figure 5b). For all reaction channels examined in this work, only one certain spin

multiplicity among triplet, quindruplet, and heptet has major contribution to a certain reaction channel. Therefore, the structural and energetic information are presented only for the spin multiplicities with the lowest free energy of the transition state, hereafter in this Article.

The free-energy profile depicted in Figure 5b shows that among all five reaction channels examined for the β-H elimination pathway the most favorable one is **CHAN-β-1**. That is, the β-H atom is most favorable to go to the O(1) site rather than other sites. For the two channels where the β-H atom goes to a Ni site, **CHAN-β-2** and **CHAN-β-6**, the latter is more favorable. That is, compared with other Ni sites, the β-H atom is relatively easy to go to the nearest Ni site [Ni(1)]. Using eq 1, one can obtain that $k_{\beta-6}/k_{\beta-1}$ is 0.132, $k_{\beta-5}/k_{\beta-1}$ is 0.0087, and the relative rates of other channels over the rate of **CHAN-β-1** are even much smaller. That is, over 88% of the β-H atoms go to the O(1) site, and ~11.5% of the β-H atoms go to the Ni(1) site, and the contributions of other channels are negligible.

By inspection of Figure 5b, it was found that **CHAN-β-1** and **CHAN-β-3** are mildly exothermic, **CHAN-β-6** is slightly endothermic, and **CHAN-β-2** and **CHAN-β-3** are mildly endothermic. This indicates that it is thermodynamically favorable for H to go to "bare" O site (such as O(2) or O(3)) rather than other sites.

3.2.2. α-H Abstraction Pathway. Although there are possibly six sites for the α-H atom to go to as indicated in Scheme 1b (**CHAN-α-p**), the transition-state structures of only three reaction channels, that is, **CHAN-α-1**, **CHAN-α-5**, and **CHAN-α-6**, were found. The other three reaction channels were not found, maybe because the Ni(2), O(3), and Ni(3) site are too far for the α-H atom compared with the Ni(1), O(1), and O(2) sites. **TS-α-p** and **PC-α-p** are denoted as the transition states and product complexes for **CHAN-α-p** (where $p = 1,5,6$), and their optimized geometries are presented in Figure 6. By inspection of the geometrical parameters shown in Figure 6, it can be seen than for **CHAN-α-1** and **CHAN-α-5**, the detachment of the H(1) atom from C(1) atom is accompanied by the decrease in the C(1)−Ni(1) bond length as well as the H(1)$\cdots$O distance. For **CHAN-α-6**, where the α-
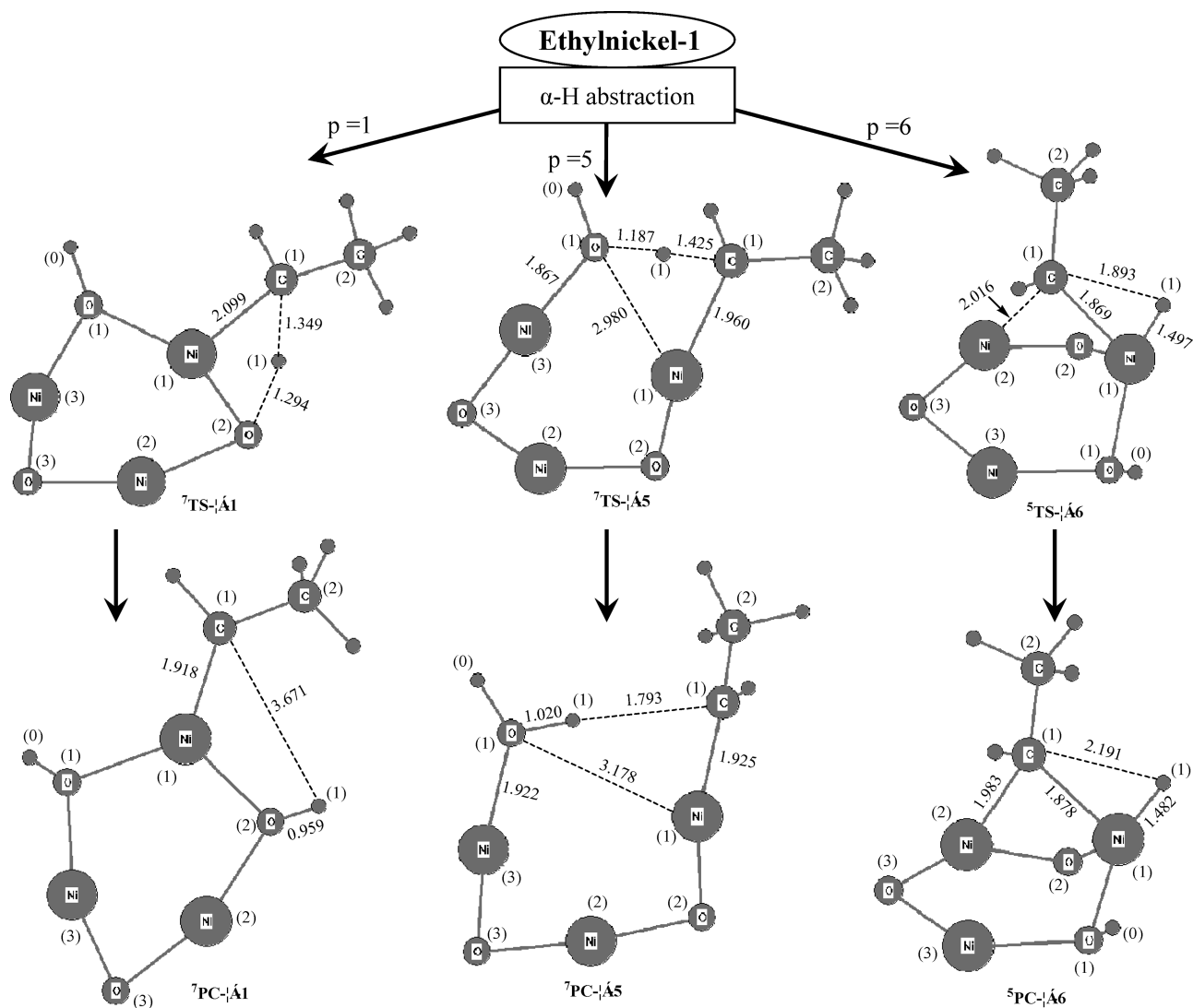
Figure 6. Optimized geometries for the transition states and product complexes for three reaction channels examined for the α-H abstraction pathway of **Ethylnickel-1**. Key distances are indicated in angstroms. The upper-left number of the notation of each structure is the spin multiplicity. See Scheme 1b as well.

H atom is abstracted by the Ni(1) site, the C(1)···H(1) distance in the transition state (**TS-α-6**) is much larger than that in **TS-α-1** or **TS-α-2**, implicating that the abstraction of the α-H atom by the α-Ni atom is much more difficult than that by the nearby O atoms. This hypothesis is supported by Figure 7a, which depicts the relative free-energy profiles of these α-H abstraction reaction channels.

As can be seen in Figure 7a, the free energy of **TS-α-6** is higher than that of **TS-α-5** for ~19 kcal/mol, whereas that of **TS-α-1** is rather close to that of **TS-α-5**. Using eq 1, one can obtain $k_{\alpha\text{-}6}/k_{\alpha\text{-}5} = 2.1 \times 10^{-5}$ and $k_{\alpha\text{-}1}/k_{\alpha\text{-}5} = 0.37$. These data mean that the α-H atom may go to either one of the nearest O atom for the α-H abstraction pathway.

3.2.4. C−C Bond Cleavage Pathway. Detachment of methyl [C(2)H$_3$] group from the methylene [C(1)H$_2$] moiety in the ethyl group leads to the C−C bond cleavage pathways for **Ethylnickel-1**, and in this work only two reaction channels, as indicated in Scheme 1c, were found. In both of reaction channels, the C−C bond cleavage pathway undergoes only at the nearest Ni [Ni(1)] site. The C(1)H$_2$ moiety has to find another site to form a new bond during the detachment of the

methyl group. The channel where a new bond formed between C(1) and Ni(2) is denoted as **CHAN-cle-1**, and the one where a new bond formed from C(1) and Ni(3) is denoted as **CHAN-cle-2**, as indicated in Scheme 1c. Figure 8 presents the optimized geometries of the transition states (**TS-cle-p**, p = 1,2) and product complexes (**PC-cle-p**) involved in **CHAN-cle-p**, and Figure 7b depicts the relative free-energy profiles for these two reaction channels. A local trigonal structure of C(1)···C(2)···Ni(1) in **TS-cle-p** with the C···C distance of ~2.1 Å, which is very similar to the reductive elimination step of Ni(terpyridine)-catalyzed cross-coupling reactions.[56] This reductive elimination step (forming C−C bond) can be considered to be the reverse step of C−C bond cleavage. As can be seen in Figure 7b, these two reaction channels have a close free energy of activation, and the **PC**s are both highly endothermic.

3.2.4. Isomerization Pathway between an Ethylnickel and an Ethoxide Species. An important issue for transition-metal-catalyzed oxidation of hydrocarbon is the type of primary species generated from the C−H bond activation step and the type of species directly responsible for the initial product
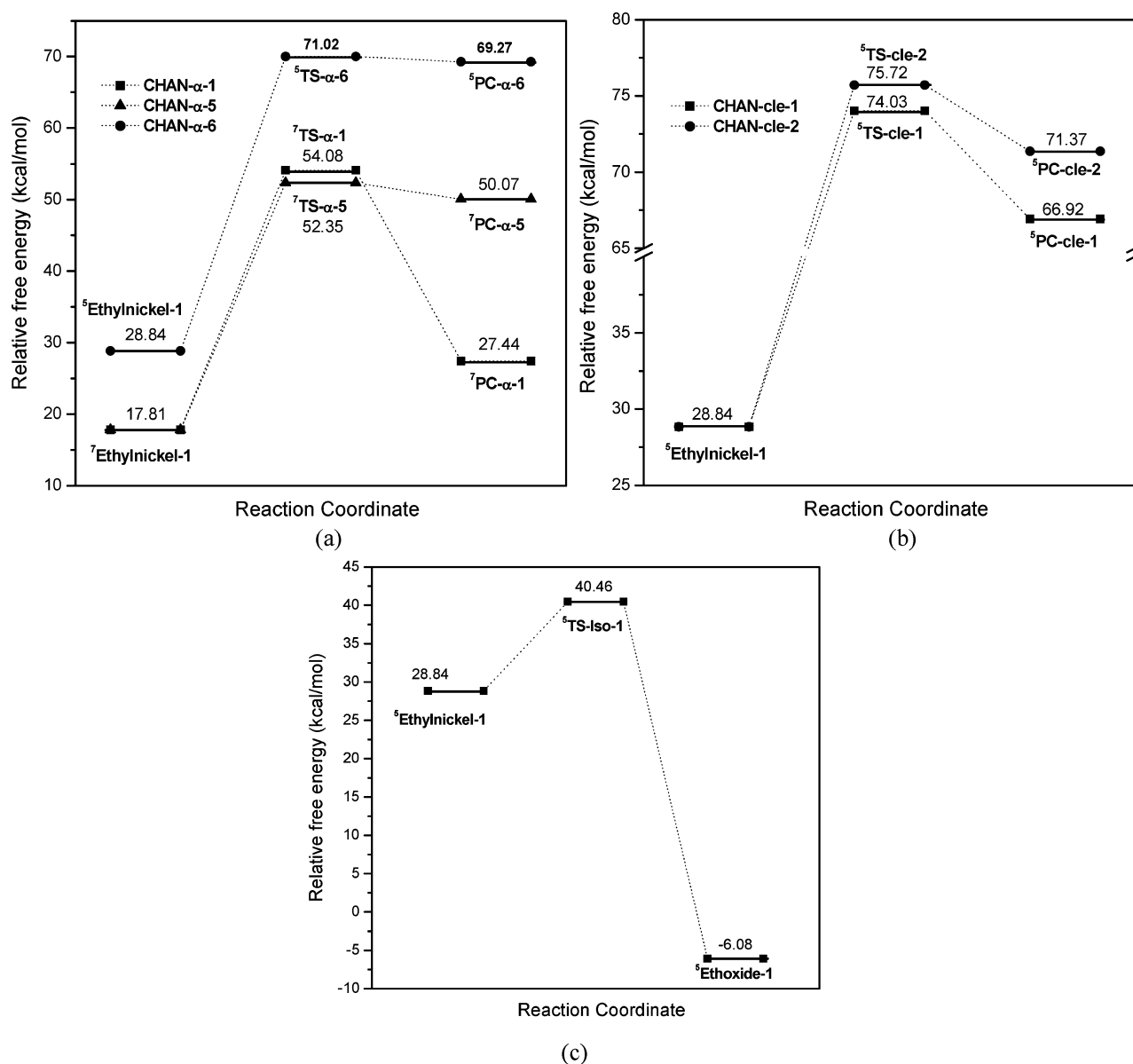
Figure 7. Relative free energy (at 873.15 K) profiles for (a) the three channels of the α-H abstraction pathway of **Ethylnickel-1**, (b) the two channels of the C−C bond cleavage pathway of **Ethylnickel-1**, and (c) the isomerization of **Ethylnickel-1** to **Ethoxide-1**. The free energy of heptet $Ni_3O_3 + C_2H_6$ is the reference.

selectivity observed in experiment. Because the alkyl group can be bounded to a metal site to form an alkylmetal or bounded to an O site to form a metal alkoxide, many concerns have been taken to the issue for whether alkylmetal or metal alkoxide is the key intermediate responsible for the initial selectivity.[2,3,57,58] Because of the short lifetime of the suggested intermediate(s), presently there are no spectroscopic data from which the structure of intermediate can be unequivocally determined. Busca and coworkers[58] have used IR to study the surface species on the Mn_3O_4, Co_3O_4, and $MgCr_2O_4$ catalysts when exposed to a reaction feed of propane and O_2, and they suggested that the intermediates of metal propoxides be plausible.

In this work, efforts have been taken on understanding how easily the above two intermediates isomerize to each other. Scheme 1d shows two reaction channels (**iso-1** and **iso-3**) for the isomerzation pathway of **Ethylnickel-1** and two channels for **Ethoxide-1** (**iso-2** and the reverse of **iso-1**). The first pictorial panel in Figure 9 shows the transition-state (**TS-iso-1**) structure for transforming **Ethylnickel-1** to **Ethxoide-1**, and the second panel in Figure 9 shows the structure of the **Ethoxide-1**. The **iso-3** channel where **Ethylnickel-1** transforms to **Ethoxide-2** was not found, which could be accounted for less positively charge of the O(1) site than that of other O sites. The free energy of **TS-iso-1** with quindruplet state is 40.5 kcal/mol (Figure 7c), and the free energy of activation for the isomerization step is 22.6 kcal/mol at 873 K. This free energy of activation corresponds to a first-order reaction rate constant of $3.9 \times 10^7 \text{ s}^{-1}$ using gas-phase model or a half-lifetime of 1.8×10^{-8} s. Even at room temperature, the free energy of activation for **Ethylnickel-1** to isomerize to **Ethoxide-1** is 18.2 kcal/mol, which corresponds to a half-life time of only 2.5 s. **Ethoxide-1** is more stable than **ethylnickel-1** by 26.1 kcal/mol lower in energy, respectively. The above energetic data indicate that in a typical alkane oxidation system where the reaction temperature is usually over 600 K, it is very difficult to capture alkylmetal
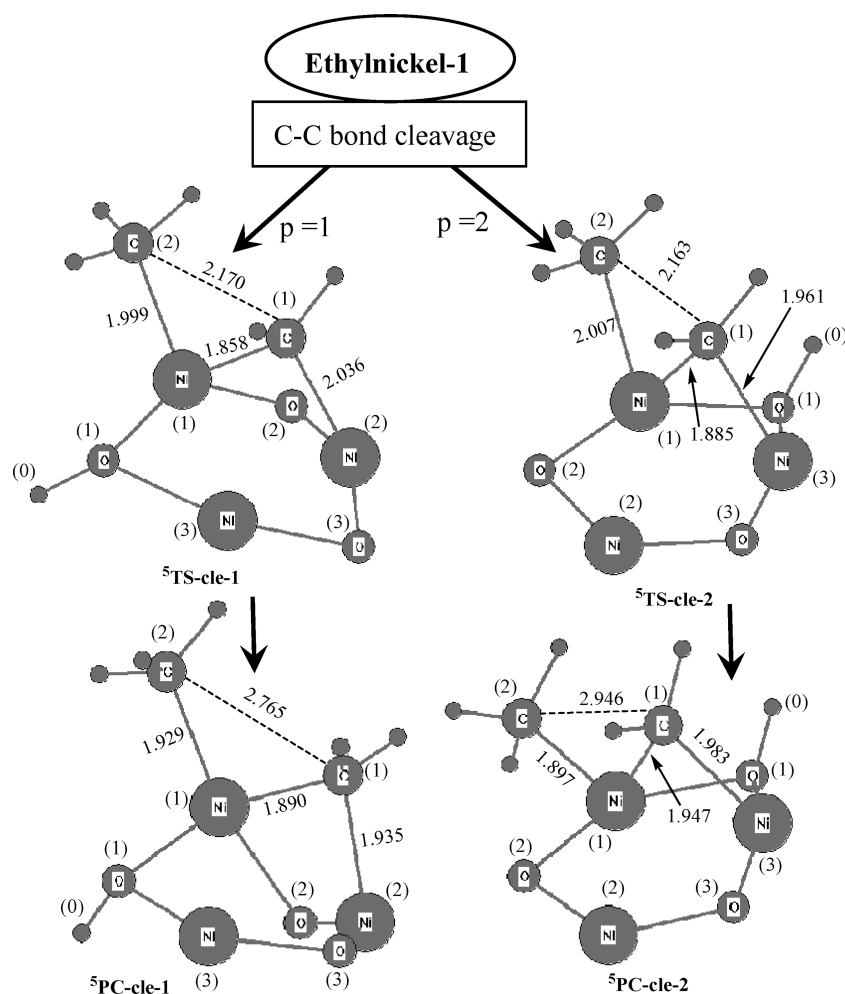
Figure 8. Optimized geometries for the transition states and product complexes for the two reaction channels examined for the C−C bond cleavage pathway of **Ethylnickel-1**. Key distances are indicated in angstroms. The upper-left number of the notation of each structure is the spin multiplicity. See Scheme 1c as well.
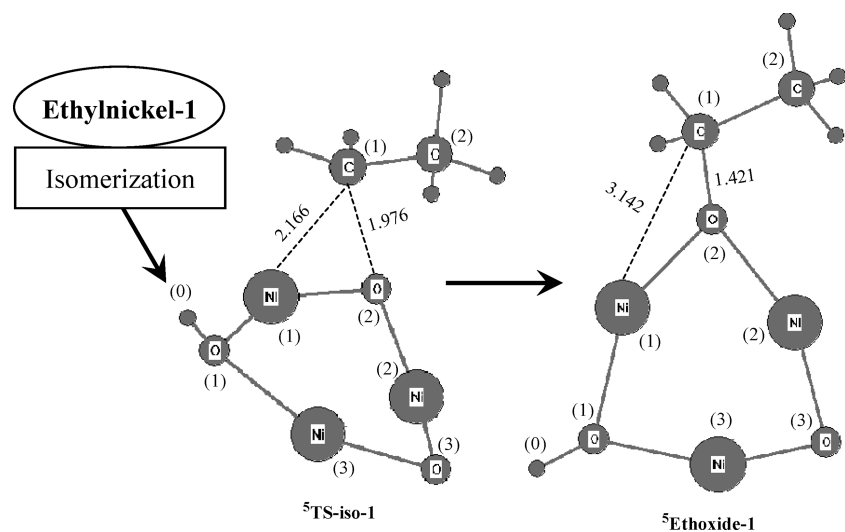
Figure 9. Optimized geometries for the transition states and product for the isomerization of **Ethylnickel-1** to **Ethoxide-1**. Key distances are indicated in angstroms. The upper-left number of the name of each structure is the spin multiplicity. See Scheme 1d as well.

species using in situ spectroscopic tools due to its short lifetime. If an alkylmetal species can be formed at room or even lower temperatures, then it would be feasible to observe it before transforming to other species.

3.2.5. Reaction Pathways of *Ethoxide-1* Species. Because the isomerization of **Ethylnickel-1** to **Ethoxide-1** is rather facile and thermodynamically favorable, it is important to explore the reaction behaviors of **Ethoxide-1** to better understand the

J
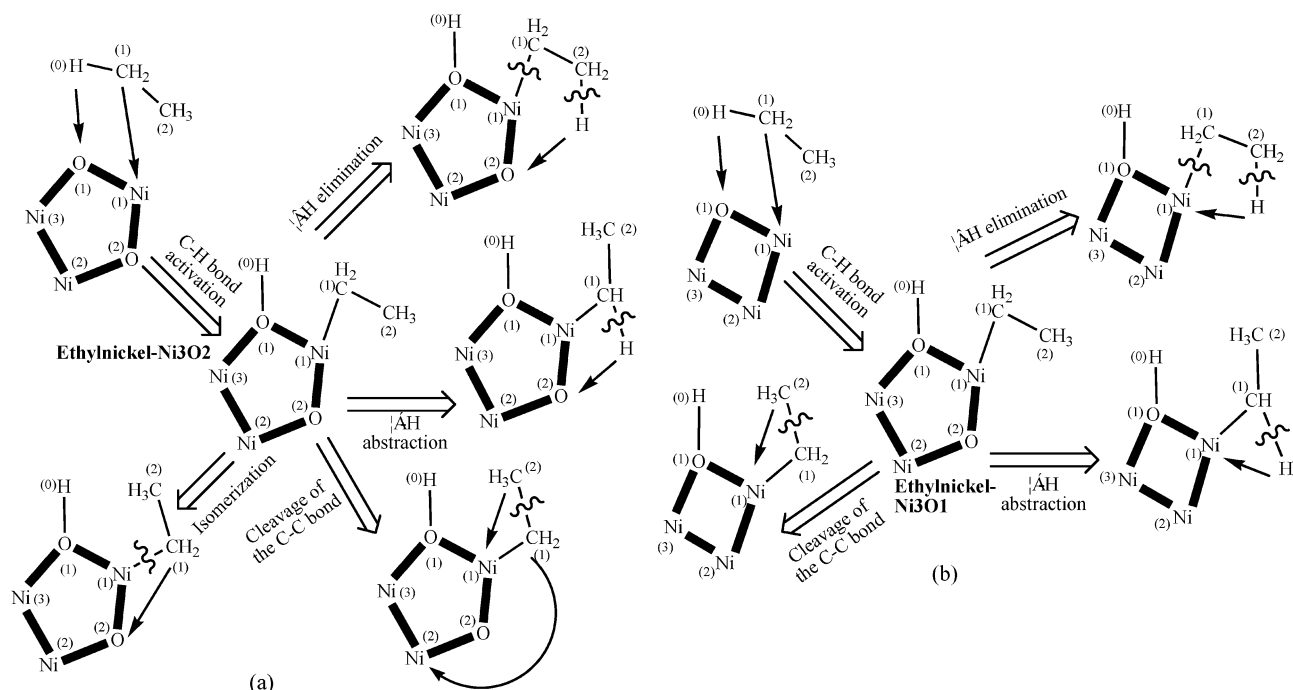
Scheme 2[a]

[a](a) Schematic diagrams for the C−H bond activation step and the four reaction pathways in the following step for the case of C_2H_6 reacting with Ni_3O_2 cluster. (b) Schematic diagrams for the C−H bond activation step and the three reaction pathways in the following step for the case of C_2H_6 reacting with Ni_3O_1 cluster. All of the optimized geometries involved in these two reactions are presented in Figure 3S for (a) and Figure 4S for (b) in the Supporting Information.

initial product selectivity. For **Ethoxide-1**, besides the β-H elimination, α-H abstraction, and C−C bond cleavage pathways, there are two isomerization pathways (reverse of **iso-1** to produce **Ethylnickel-1** and **iso-2** to produce **Ethylnickel-2** as indicated in Scheme 1d). To emphasis the main points of this work, we present here only the reaction channel with the lowest free energy for each reaction pathway. The optimized geometries for the two isomerization pathways and their corresponding free-energy profiles are given in Figures 1S and 2S, and those for the other three pathways are given in Figures 3S and 4S in the Supporting Information.

The product preceded by **TS-β-ethox** is $Ni_3O(OH)_2$ and ethylene. The product preceded by **TS-α-ethox** is an adsorbing acetaldehyde, as proposed elsewhere.[36] The product preceded by **TS-cle-ethox** is methylnickel and an adsorbing form-aldehyde molecule. By putting the free-energy profiles depicted in Figures 2S and 4S together, one can see that for **Ethoxide-1** the most easily undergoing pathway is C−C bond cleavage, and the second most easily undergoing one is to isomerize to **Ethylnickel-2**. This is dramatically different from the reaction behavior of **Ethylnickel-1**. The relative rate of these two pathways $k_{iso-2}/k_{cle} = 0.15$ using eq 1. The β-H elimination pathway of ethoxide to afford ethylene is a much slower process as $k_\beta/k_{cle} = 4.3 \times 10^{-4}$. The reaction rate of the α-H abstraction pathway is even lower. The above data show that when an ethoxide intermediate is formed, it is unlikely to produce ethylene (with β-H elimination pathway).

3.3. Ethylene Selectivity for C_2H_6 Reacting with Ni_3O_3. Putting together all free-energy profiles in Sections 3.1 and 3.2, the selectivity of ethylene (S_{C2}) can be calculated for the reaction of C_2H_6 with Ni_3O_3 cluster. In Section 3.1, it has been demonstrated that producing **Ethylnickel-1** is a main pathway for the C−H bond activation step. In Section 3.2, it has been

demonstrated that **Ethylnickel-1** may undergo four reaction pathways, α-H abstraction, β-H elimination, C−C bond cleavage, and isomerization to form Ethoxide-1. The result described in Section 3.2.5 shows that if **Ethylnickel-1** is converted to **Ethoxide-1**, then it is not likely to form ethylene. Therefore, the sum of rate constants of all pathways that produce ethylene, denoted as k_A, equals k_β, and the sum of rate constants of all pathways that do not produce ethylene, denoted as k_B, equals $k_\alpha + k_{cle} + k_{iso-1}$. Then, S_{C2} for C_2H_6 reacting with Ni_3O_3 cluster can be calculated by

$$
\begin{aligned}
S_{C2} &= k_A/(k_A + k_B) \\
&= \frac{k_\beta}{k_\beta + k_\alpha + k_{cle} + k_{iso-1}} \\
&= [\exp(-G_{TS-\beta}/RT)]/[\exp(-G_{TS-\beta}/RT) \\
&\quad + \exp(-G_{TS-\alpha}/RT) + \exp(-G_{TS-cle}/RT) \\
&\quad + \exp(-G_{TS-iso-1}/RT)]
\end{aligned}
\tag{2}
$$

where G_{TS} is the free energy for a transition state relative to an arbitrary reference. When $T = 873.15$ K, S_{C2} is calculated to be 37.0%, which is 36.2% at 823.15 K upon employing eq 2. The G_{TS} data for all four pathways examined for **Ethylnickel-1** can be seen in Figures 5b and 7. The relatively low selectivity of ethylene is mainly due to a slightly higher $G_{TS-\beta-1}$ than $G_{TS-iso-1}$. The contribution of the α-H abstraction pathway is small compared with that of the β-H elimination pathway, as $k_\alpha/k_\beta = 0.047$ at 873.15 K, and the contribution of the C−C bond cleavage pathway is unlikely to undergo, as $k_{cle}/k_\beta = 1.8 \times 10^{-7}$ at 873.15 K.

3.4. C$_2$H$_6$ Reacting with Ni$_3$O$_2$ and Ni$_3$O$_1$ Clusters. The Ni$_3$O$_2$ and Ni$_3$O$_1$ clusters were use in this work to model the active sites when exposed to the reaction feed with a fuel-rich atmosphere. (The flow rate of C$_2$H$_6$ is larger than that of O$_2$ for ODHE for instance.)[31–41] The reactions of C$_2$H$_6$ with Ni$_3$O$_2$ and Ni$_3$O$_1$ were investigated by examination of similar reaction steps and pathways, as examined for the reaction of C$_2$H$_6$ with Ni$_3$O$_3$. The primary reaction pathway for the C–H bond activation step (first step) and the primary reaction channel for different pathways in the second step for both of these two reactions are indicated in Scheme 2. The optimized geometries of the species involved in Scheme 2 are presented in Figures 5S and 6S in the Supporting Information.

For the C–H bond activation step undergoing with a concerted mechanism on an Ni$_3$O$_2$ cluster, C(1) may be bound to either Ni(1) or Ni(2) site, as indicated in Figure 1b. It was found that the reaction channel with lower free energy of activation for the C–H bond activation is to undergo with the Ni(1) site (Scheme 2a and the left two panels in Figure 5S in the Supporting Information). The product for the C–H bond activation step is denoted as **Ethylnickel-Ni$_3$O$_2$**. In the second step, **Ethylnickel-Ni$_3$O$_2$** may undergo four pathways, the same as those described in the **Ethylnickel-1** case (Scheme 1). Figure 10 depicts the corresponding free-energy profiles for the first and second steps. It can be seen that the free energy of the transition state for the β-H elimination pathway is slightly
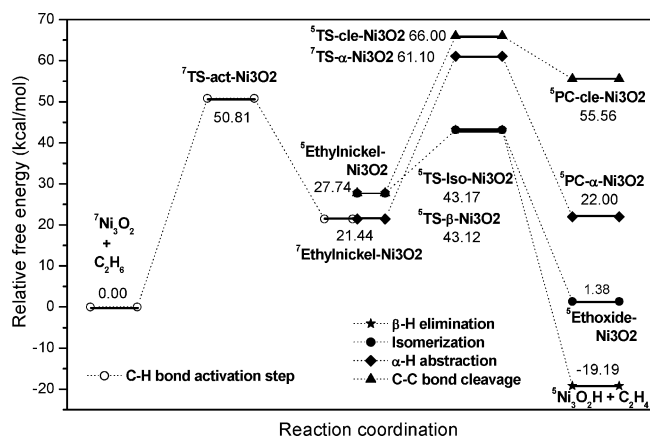
Figure 10. Free-energy profiles (at 873.15 K) for the C–H bond activation step (○), and four pathways after the C–H bond activation step for β-H elimination (★), α-H elimination (◆), C–C bond cleavage (▲), and isomerization (●), for C$_2$H$_6$ reacting with Ni$_3$O$_2$. Note that the free energies of TSs for β-H elimination and isomerization are so close to each other that the corresponding lines are nearly overlapped with each other.

smaller than that for the isomerization pathway, and those for α-H elimination and C–C bond cleavage pathways are much larger.

The C–H bond activation step (Scheme 2b and the left two panels in Figure 6S in the Supporting Information) undergoes a similar mechanism as in the cases of Ni$_3$O$_3$ and Ni$_3$O$_2$. The product of this step is denoted as **Ethylnickel-Ni$_3$O$_1$**. The free energy of activation (46.2 kcal/mol at 873.15 K, see Figure 11) for the Ni$_3$O$_1$ case is slightly less than those in the cases of Ni$_3$O$_3$ (47.1 kcal/mol) and Ni$_3$O$_2$ (50.8 kcal/mol). For second step, because there is no "bare" O atom in the neighbor of the C$_2$H$_5$ moiety of **Ethylnickel-Ni$_3$O$_1$**, the isomerization pathway to afford ethoxide species is unlikely and thus is not
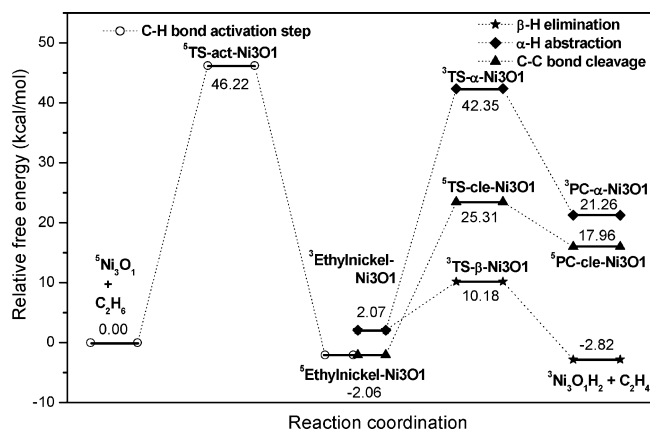
Figure 11. Free-energy profiles (at 873.15 K) for the C–H bond activation step (in open cycles) and three pathways after the C–H bond activation step for β-H elimination (★), α-H elimination (◆), and C–C bond cleavage (▲) for C$_2$H$_6$ reacting with Ni$_3$O$_1$.

considered here, and the β-H and α-H atoms cannot go to an O(2) site like those in Ni$_3$O$_3$ and Ni$_3$O$_2$ cases. Therefore, the reaction channel of the β-H elimination pathway likes the **CHAN-β-6** in the Ni$_3$O$_3$ case. (See $p = 6$ in Scheme 1a and in Figure 4.) The reaction channel of the α-H abstraction pathway likes the **CHAN-α-6** in the Ni$_3$O$_3$ case. (See $p = 6$ in Scheme 1b and in Figure 6.) Figure 11 also depicts the free-energy profiles for these three reaction pathways. It can be seen that the reaction barrier required by β-H elimination is much less than those for the α-H abstraction and C–C bond cleavage pathways.

By applying the free-energy data for these two reaction (Figures 10 and 11) to eq 2, one can obtain the selectivity of ethylene (S_{C2}) for both reactions. The S_{C2} is 50.7% at 873.15 K and 50.5% at 823.15 K for C$_2$H$_6$ reacting with Ni$_3$O$_2$. The increase in S_{C2} for the Ni$_3$O$_2$ case compared with the Ni$_3$O$_3$ case is accounted for the increase in relative reaction rate of the β-H elimination pathway over the isomerization pathway. For the case of C$_2$H$_6$ reacting with Ni$_3$O$_1$, the contributions of α-H abstraction and C–C bond cleavage are trivial, as $k_\alpha/k_\beta = 8.9 \times 10^{-9}$ and $k_{cle}/k_\beta = 4.7 \times 10^{-4}$, and the absence of isomerization leads to very high S_{C2} of >99%.

3.5. Further Discussion on the Mechanism and Catalyst Design For ODH Reaction of Alkanes. Sections 3.1–3.4 present a detailed structural and energetic investigation for the reactions of C$_2$H$_6$ with Ni$_3$O$_x$ ($x = 1,2,3$) clusters, which model the small NiO·Ni$_y$ clusters[36] in a supported catalyst with different oxidation states of nickel element. By inspection of all free-energy profiles in this Article (Figures 3, 5, 7, 10, and 11 and Figures 2S and 4S of the Supporting Information), one may found that the free energy of activation required by the first step is higher than that by the second step for all cases of different x values, indicating that the first step is rate-determining according to the energetic span model.[59–61] However, the second step determines the product selectivity instead of the first step. The selectivity of ethylene calculated by employing eq 2 for a certain reaction increases from 37.0% when $x = 3$ to 50.7% when $x = 2$ and to over 99% when $x = 1$. The increasing S_{C2} mainly accounts for the increase in relative rate of the β-H elimination pathway over the isomerization pathway. This implicates, that the reaction behavior of the intermediate produced from the first step as well as the selectivity of ethylene is sensitively dependent on the oxidation

state of the active sites. A more reduced state of the nickel component may benefit the production of alkene for the ODH reactions. An ideal ODH catalyst could have a high concentration of active sites that produce alkylmetal species in the first step and block the isomerization pathway in the second step.

In our previous study, we have found that on the zeolite-Y supported nickel oxide catalyst[35] the initial selectivity of ethylene (S_0) from the ethane oxidation ranges from 90 to 96% at the temperature of 550−600 °C. S_0 was obtained from the plot of the selectivity to ethylene with the conversion of ethane by the extrapolation of the conversion to 0. According to the generally accepted reaction scheme (Scheme 3a)[5,57] for ODH reactions, the selectivity of alkene at low conversion of alkane mainly depends on the k_1/k_2 ratio, whereas at higher conversions of alkane, the observed selectivity of alkene is

Scheme 3. Simple Reaction Networks of Oxidative Dehydrogenation of Alkanes to Alkenes: (a) General Scheme and (b) Initial Steps in the Mar−van Krevenlen Mechanism
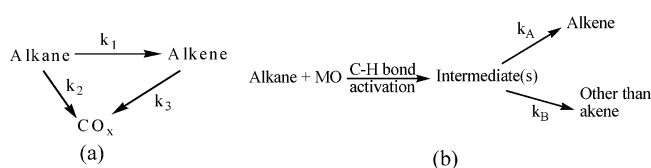
associated with the ratio $k_1/(k_2 + k_3)$. When the conversion is extrapolated to 0, the corresponding selectivity can be calculated as: $S_0 = k_1/(k_1 + k_2)$. However, on the molecular level, the conversion of alkane either to alkene or to CO_x may contain several steps that are not well understood.

The ODH catalysts can be divided into three categories,[8] that is, (1) catalysts based on reducible metal oxides, (2) noble-metal-based catalysts, primarily Pt-based ones, and (3) catalysts that generate radicals to initiate homogeneous reactions in the gas phase. (These are typically alkali earth and rear earth metal oxides.) The first category is the most extensively studied, and the reaction mechanism is generally believed to be the Mars−van Krevenlen mechanism involving a key step of C−H bond activation.[2] As illustrated in Scheme 3b, if the primary intermediate of the C−H bond activation step is known, then k_1/k_2 is associated with the relative rate of the pathways that produce alkene and that do not produce alkene, or $k_1/k_2 = k_A/k_B$. (See Section 3.3.) Therefore, S_0 should be equal to S_{C2} (eq 2) if only one type of active site exists in the supported catalyst. However, there can be various types of active site on a common catalyst even if there is only one type of metal in the active component. The experimental data[35] implicate that, more than 90% of the intermediate(s) from the C−H bond activation step is converted to ethylene, and a small portion is converted to species other than ethylene. The computational result in this work shows that the selectivity of ethylene is highly dependent on the degree of reduction of the metal oxide clusters. Therefore, it is reasonable to anticipate that in the real catalyst the C−H bond activation mainly undergoes on a relatively more reduced site rather than on more oxidized sites. This is consistent with the result that the free energy of activation needed for the C−H bond activation step in the Ni_3O_1 case is lower than those in the Ni_3O_2 and Ni_3O_3 cases. (See Figures 3, 10, and 11.)

Because of high demand of the computational resource in calculating metal oxide nanoclusters with different spin multiplicity, the incorporation of a support into the Ni_3O_x clusters was not examined in this Article. However, because support effect is also important to the catalytic performance of a catalyst, a further DFT study of the support effect is desirable for a deeper understanding of the ODH mechanism. The work along this avenue is now being performed in our group.

4. CONCLUSIONS

The following conclusions on the reactions of C_2H_6 with Ni_3O_x (x = 1,2,3) clusters can be made:

(1) For the case of Ni_3O_3, the C−H bond activation step may undergo with three pathways, with concerted or stepwise mechanisms. The pathway with concerted mechanism where the C and H atoms on the C−H bond attack two different sites is the most favorable pathway. The main product produced from the C−H bond activation step is **Ethylnickel-1**.

(2) Eleven reaction channels were examined to understand the reaction behavior of **Ethylnickel-1**: five for the β-H elimination pathways to afford ethylene, three for the α-H abstraction pathway, two for the C−C bond cleavage pathway, and one for the isomerization pathway to produce **Ethoxide-1**. The most favorable two pathways are isomerization and β-H elimination.

(3) The most favorable pathway for **Ethoxide-1** is to undergo C−C bond cleavage, resulting in a situation that if **Ethylnickel-1** undergoes isomerization pathway, then ethylene is unlikely to be produced. The selectivity of ethylene (S_{C2}) can be calculated from the relative rate of β-H elimination over the sum of rates for all pathways for **Ethylnickel-1**.

(4) S_{C2} for C_2H_6 reacting with Ni_3O_3 is ∼37%, which is slightly over 50% for the Ni_3O_2 case and is over 99% for the Ni_3O_1 case at 823−873 K. The high S_{C2} for the Ni_3O_1 case is due to the absence of bare O atom nearby the α-Ni site, which makes the isomerization pathway unavailable.

This work provides a deep insight into the reaction mechanism for ODH reactions catalyzed by Ni-based catalysts. The conclusion that S_{C2} increases with decreasing x value in the Ni_3O_x cluster may provide an important clue for designing ODHE catalysts giving high ethylene selectivity.

■ ASSOCIATED CONTENT

⑤ Supporting Information

Optimized geometries, relative free energies, and Cartesian coordinates for all the optimized structures at the B3LYP/BS1 level of theory in the manuscript. This material is available free of charge via the Internet at http://pubs.acs.org.

■ AUTHOR INFORMATION

Corresponding Author

*E-mail: hatrick2009@upc.edu.cn.

■ ACKNOWLEDGMENTS

M

dx.doi.org/10.1021/jp2088274 | J. Phys. Chem. C XXXX, XXX, XXX−XXX

■ REFERENCES

(1) Cavani, F.; Ballarini, N.; Cericola, A. *Catal. Today* **2007**, *127*, 113−131.

(2) Grabowski, R. *Catal. Rev.: Sci. Eng.* **2006**, *48*, 199−268.

(3) Kung, H. H. *Adv. Catal.* **1994**, *40*, 1−38.

(4) Tsilomelekis, G.; Christodoulakis, A.; Boghosian, S. *Catal. Today* **2007**, *127*, 139−147.

(5) Argyle, M. D.; Chen, K.; Bell, A. T.; Iglesia, E. *J. Phys. Chem. B* **2002**, *106*, 5421−5427.

(6) Klose, F.; Joshi, M.; Hamel, C.; Seidel-Morgenstern, A. *Appl. Catal., A* **2004**, *260*, 101−110.

(7) Heracleous, E.; Lemonidou, A. A.; Lercher, J. A. *Appl. Catal., A* **2004**, *264*, 73−80.

(8) Cavani, F.; Trifiro, F. *Catal. Today* **1999**, *51*, 561−580.

(9) You, H. *Pet. Sci. Technol.* **2005**, *23*, 1441−1452.

(10) Henning, D. A.; Schmidt, L. D. *Chem. Eng. Sci.* **2002**, *57*, 2615−2625.

(11) Christodoulakis, A.; Machli, M.; Lemonidou, A. A.; Boghosian, S. *J. Catal.* **2004**, *222*, 293−306.

(12) Rozanska, X.; Sauer, J. *J. Phys. Chem. A* **2009**, *113*, 11586−11594.

(13) Kuzmin, I. V.; Zhidomirov, G. M.; Solkan, V. N.; Kazanskii, V. B. *Kinet. Catal.* **2009**, *50*, 752−759.

(14) Rozanska, X.; Kondratenko, E. V.; Sauer, J. *J. Catal.* **2008**, *256*, 84−94.

(15) Dai, G.-L.; Liu, Z.-P.; Wang, W.-N.; Lu, J.; Fan, K.-N. *J. Phys. Chem. C* **2008**, *112*, 3719−3725.

(16) Fu, H.; Liu, Z.-P.; Li, Z.-H.; Wang, W.-N.; Fan, K.-N. *J. Am. Chem. Soc.* **2006**, *128*, 11114−11123.

(17) Wannakao, S.; Boekfa, B.; Khongpracha, P.; Probst, M.; Limtrakul, J. *ChemPhysChem* **2010**, *11*, 3432−3438.

(18) Rozanska, X.; Fortrie, R.; Sauer, J. *J. Phys. Chem. C* **2007**, *111*, 6041−6050.

(19) Nguyen, N. H.; Tran, T. H.; Nguyen, M. T.; Le, M. C. *Int. J. Quantum Chem.* **2010**, *110*, 2653−2670.

(20) Ganduglia-Pirovano, M. V.; Popa, C.; Sauer, J.; Abbott, H.; Uhl, A.; Baron, M.; Stacchiola, D.; Bondarchuk, O.; Shaikhutdinov, S.; Freund, H.-J. *J. Am. Chem. Soc.* **2010**, *132*, 2345−2349.

(21) Cheng, M.-J.; Chenoweth, K.; Oxgaard, J.; Van Duin, A.; Goddard, W. A. III. *J. Phys. Chem. C* **2007**, *111*, 5115−5127.

(22) Govindasamy, A.; Muthukumar, K.; Yu, J.; Xu, Y.; Guliants, V. V. *J. Phys. Chem. C* **2010**, *114*, 4544−4549.

(23) Xu, X.; Faglioni, F.; Goddard, W. A. III. *J. Phys. Chem. A* **2002**, *106*, 7171−7176.

(24) Vajda, S.; Pellin, M. J.; Greeley, J. P.; Marshall, C. L.; Curtiss, L. A.; Ballentine, G. A.; Elam, J. W.; Catillon-Mucherie, S.; Redfern, P. C.; Mehmood, F.; et al. *Nat. Mater.* **2009**, *8*, 213−216.

(25) Chen, M. S.; Goodman, D. W. *Science* **2004**, *306*, 252−255.

(26) Schimmoeller, B.; Jiang, Y.; Pratsinis, S. E.; Baiker, A. *J. Catal.* **2010**, *274*, 64−75.

(27) Capek, L.; Adam, J.; Grygar, T.; Bulanek, R.; Vradman, L.; Kosova-Kucerova, G.; Cicmanec, P.; Knotek, P. *Appl. Catal., A* **2008**, *342*, 99−106.

(28) Chao, Z.-S.; Ruckenstein, E. *J. Catal.* **2004**, *222*, 17−31.

(29) Christodoulakis, A.; Heracleous, E.; Lemonidou, A. A.; Boghosian, S. *J. Catal.* **2006**, *242*, 16−25.

(30) Watson, R. B.; Ozkan, U. S. *J. Catal.* **2000**, *191*, 12−29.

(31) Solsona, B.; Lopez Nieto, J. M.; Concepcion, P.; Dejoz, A.; Ivars, F.; Vazquez, M. I. *J. Catal.* **2011**, *280*, 28−39.

(32) Heracleous, E.; Lemonidou, A. A. *J. Catal.* **2010**, *270*, 67−75.

(33) Sakitani, K.; Nakamura, K.-i.; Ikenaga, N.-o.; Miyake, T.; Suzuki, T. *J. Jpn. Pet. Inst.* **2010**, *53*, 327−335.

(34) Savova, B.; Loridant, S.; Filkova, D.; Millet, J. M. M. *Appl. Catal., A* **2010**, *390*, 148−157.

(35) Lin, X.; Poeppelmeier, K. R.; Weitz, E. *Appl. Catal., A* **2010**, *381*, 114−120.

(36) Lin, X.; Hoel, C. A.; Sachtler, W. M. H.; Poeppelmeier, K. R.; Weitz, E. *J. Catal.* **2009**, *265*, 54−62.

(37) Heracleous, E.; Lemonidou, A. A. *J. Catal.* **2006**, *237*, 162−174.

(38) Heracleous, E.; Lee, A. F.; Wilson, K.; Lemonidou, A. A. *J. Catal.* **2005**, *231*, 159−171.

(39) Nakamura, K.-I.; Miyake, T.; Konishi, T.; Suzuki, T. *J. Mol. Catal. A: Chem.* **2006**, *260*, 144−151.

(40) Zhang, X.; Gong, Y.; Yu, G.; Xie, Y. *J. Mol. Catal. A: Chem.* **2002**, *180*, 293−298.

(41) Zhang, X.; Liu, J.; Jing, Y.; Xie, Y. *Appl. Catal., A* **2003**, *240*, 143−150.

(42) Fukudome, K.; Kanno, A.; Ikenaga, N.-o.; Miyake, T.; Suzuki, T. *Catal. Lett.* **2011**, *141*, 68−77.

(43) Li, J.-H.; Wang, C.-C.; Huang, C.-J.; Sun, Y.-F.; Weng, W.-Z.; Wan, H.-L. *Appl. Catal., A* **2010**, *382*, 99−105.

(44) Becke, A. D. *Phys. Rev. A* **1988**, *38*, 3098−3100.

(45) Lee, C.; Yang, W.; Parr, R. G. *Phys. Rev. B* **1988**, *37*, 785−789.

(46) Becke, A. D. *J. Chem. Phys.* **1993**, *98*, 5648−5653.

(47) Pidko, E. A.; Hensen, E. J. M.; Van Santen, R. A. *J. Phys. Chem. C* **2007**, *111*, 13068−13075.

(48) Frisch, M. J.; Trucks, G. W.; Schlegel, H. B.; Scuseria, G. E.; Robb, M. A.; Cheeseman, J. R.; Montgomery, J. A., Jr.; Vreven, T.; Kudin, K. N.; Burant, J. C.et al. *Gaussian 03*, revision C.02; Gaussian, Inc.: Wallingford, CT, 2004.

(49) Ess, D. H.; Gunnoe, T. B.; Cundari, T. R.; Goddard, W. A. III; Periana, R. A. *Organometallics* **2010**, *29*, 6801−6815.

(50) Cundari, T. R.; Vaddadi, S. *Inorg. Chim. Acta* **2004**, *357*, 2863−2869.

(51) Biswas, B.; Sugimoto, M.; Sakaki, S. *Organometallics* **2000**, *19*, 3895−3908.

(52) Kurnaz, E.; Fellah, M. F.; Onal, I. *Microporous Mesoporous Mater.* **2010**, *138*, 68−74.

(53) Nykänen, L.; Honkala, K. *J. Phys. Chem. C* **2011**, *115*, 9578−9586.

(54) McMaster, M. C.; Arumainayagam, C. R.; Madix, R. J. *Chem. Phys.* **1993**, *177*, 461−472.

(55) Balcells, D.; Maseras, F. *New. J. Chem.* **2007**, *31*, 334−343.

(56) Lin, X.; Phillips, D. L. *J. Org. Chem.* **2008**, *73*, 3680−3688.

(57) Blasco, T.; Löpez Nieto, J. M. *Appl. Catal., A* **1997**, *157*, 117−142.

(58) Busca, G.; Finocchio, E.; Lorenzelli, V.; Ramis, G.; Baldi, M. *Catal. Today* **1999**, *49*, 453−465.

(59) Kozuch, S.; Amatore, C.; Jutand, A.; Shaik, S. *Organometallics* **2005**, *24*, 2319−2330.

(60) Kozuch, S.; Shaik, S. *J. Am. Chem. Soc.* **2006**, *128*, 3355−3365.

(61) Kozuch, S.; Shaik, S. *Acc. Chem. Res.* **2011**, *44*, 101−110.